AIP | Journal of Applied Physics

An x-ray study of diffusion in the Cu-Ag system

J. Unnam and C. R. Houska

Citation: Journal of Applied Physics **47**, 4336 (1976); doi: 10.1063/1.322435
View online: http://dx.doi.org/10.1063/1.322435
View Table of Contents: http://scitation.aip.org/content/aip/journal/jap/47/10?ver=pdfcov
Published by the AIP Publishing

An x-ray study of diffusion in the Cu-Ag system

J. Unnam and C. R. Houska

Department of Materials Engineering, Virginia Polytechnic Institute and State University, Blacksburg, Virginia 24061

(Received 22 March 1976)

The interdiffusion coefficients for both solid phases of the Ag-Cu system have been determined from x-ray diffraction and electron microprobe data. Specimens containing 3.2 μm of Ag on a (111)-oriented Cu crystal were used for the x-ray studies, while a 15-μm deposit of Ag was used for the probe specimens. Composition profiles for each phase were obtained from the x-ray intensity bands and a new iterative one-dimensional model was applied to determine the composition-dependent diffusion coefficients. The average diffusion coefficients for both phases are nearly equal at about 10^{-10} cm^2/sec at 750°C, the diffusion temperature. Also, the solubility for the Ag-rich phase is about three times the solubility for the Cu-rich phase. These conditions result in interface reversal, i.e., the interface first moves into the substrate and later moves toward the free surface. Structural damage resulting from atomic diffusion was found to be much smaller for the Ag-Cu system than for other single-phase Cu-base specimens that have been examined. Both crystal misorientation (tilt) and subgrains are formed as a result of diffusion. The subgrain shape in the plating depends upon the ratio of the thickness to the initial grain size of the plating.

PACS numbers: 66.30.Fq, 61.10.Fr, 68.50.+j, 64.80.Gd

I. INTRODUCTION

X-ray diffraction has been used to study volume diffusion[1–5] and grain-boundary diffusion[6] in single-phase systems with diffusion zones ranging from about 3 to 8 μm. The approach is nondestructive and is also capable of giving information on the defect structures generated by solid-state diffusion. In this investigation, a two-phase system is studied with 3.2 μm of Ag deposited onto a Cu single crystal. Although composition profiles are obtained directly from the x-ray diffraction data, a diffusion model is required if the interdiffusion coefficient is to be obtained. An iterative one-dimensional model was developed in the preceding paper to treat this system as well as other two-phase systems.[7] This can be applied to the boundary conditions associated with finite or semifinite planar systems, and the more general case which allows the interdiffusion coefficient to vary with composition. The Cu-Ag system is used to demonstrate this new method of evaluating diffusion coefficients.

II. DIFFRACTION EQUATIONS

The diffraction equations are written for an epitaxial deposition on a planar single-crystal substrate. Conventional reflection geometry is assumed with the angle of incidence of the x-ray beam equal to the angle of reflection as an average condition. An x-ray beam of cross-sectional area A_0 with an angle of incidence θ_m, irradiates a surface area given by

$$A_m = A_0/\sin\theta_m \tag{1}$$

and continues into the sample, forming an oblique column. This is illustrated in Fig. 1 where the plane 2-3 represents a limit such that material situated below this plane does not contribute a detectable signal. The maximum path length 1-2-5 depends upon the average linear absorption coefficient as well as on θ_m. Various imaginary thin sections are illustrated with each having a slightly different average composition. The incident and diffracted beams associated with an element at a depth Y_m is reduced by a factor

$$\exp\left(-\frac{2\langle\mu\rangle_m Y_m}{\sin\theta_m}\right), \tag{2}$$

where $\langle\mu\rangle_m$ is the average linear absorption coefficient for all material between the surface and a plane at a depth Y_m. Equations (1) and (2) are combined into a single expression defined as the effective volume

$$V^g_{me} = gA_m \exp\left(-\frac{2\langle\mu\rangle_m Y_m}{\sin\theta_m}\right)\Delta Y. \tag{3}$$

An orientation factor "g" has been introduced to allow for large misorientations in each crystalline material. It represents the volume fraction of deposit within the measurement range (±4°) for a specified reflection plane (hkl), and it is assumed that g does not vary with Y within the surface deposit or substrate. Under these conditions, the kinematic integrated intensity can be written in terms of the effective volume

$$P_m = I_0 Q_m V^g_{me}, \tag{4}$$

where I_0 is the intensity of the incident beam and Q_m the reflectivity per unit volume

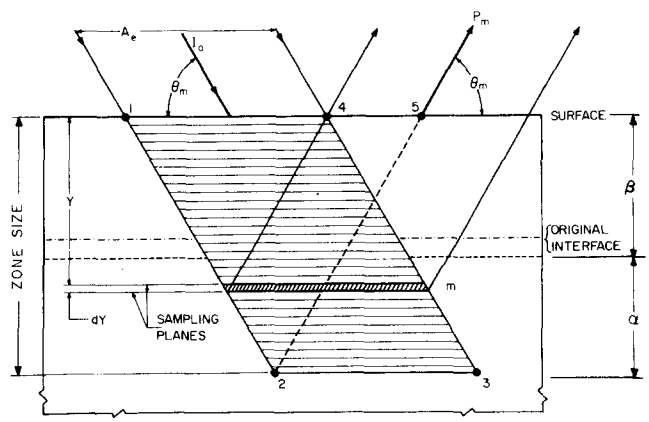

FIG. 1. Cross section of specimen, illustrating irradiated β and α regions. two sampling planes separated by dY at a distance Y. section of composition m, zone size. and incident and diffracted beams.

$$Q_m = \frac{7.94\times10^{-26}\lambda^3}{V_m^2}\left(\frac{1+\cos^2 2\alpha\cos^2 2\theta_m}{\sin 2\theta_m(1+\cos^2 2\alpha)}\right)F_m^2\exp(-2M_m) \tag{5}$$

in cgs units. The following terms vary with the composition of the diffracting element: the volume of the unit cell V_m, the structure factor F_m, and the Debye-Waller factor $\exp(-2M_m)$. λ is the x-ray wavelength and α is the Bragg angle for the monochromator.

For diffused samples having only a one-dimensional variation in composition, Eq. (4) is summed over all sections m, i.e.,

$$P_B = I_0 A_0 g \Delta Y \sum_m Q_m \left[\exp\left(-\frac{2\langle\mu\rangle_m Y_m}{\sin\theta_m}\right)\right](\sin\theta_m)^{-1}. \tag{6}$$

Summing leads to a range of intensity over 2θ since there is a different Bragg angle for each composition. The over-all distribution is defined as an intensity band.

Equation (6) can be readily summed by integrating provided both the initial plating and substrate are homogeneous phases parallel to the free surface giving

$$P_f = I_0 A_0 Q_f \frac{g_f}{2\mu_f}\left[1-\exp\left(-\frac{2\mu_f G_t}{\sin\theta_f}\right)\right], \tag{7}$$

where P_f is the integrated intensity of the surface film or plating, and G_t is its thickness. Similarly, the integrated intensity of the substrate is

$$P_s = I_0 A_0 Q_s \frac{g_s}{2\mu_s}\exp\left(-\frac{2\mu_f G_t}{\sin\theta_s}\right). \tag{8}$$

The last term allows for absorption of the incident and diffracted beams within the plating. The ratio of Eq. (7) to Eq. (8) from two orders is used to determine g_f/g_s and G_t. Both are important parameters in x-ray studies of diffusion.

III. COMPUTER SIMULATION OF INTENSITY SUBBANDS

If it is assumed that the composition profile is known, an intensity band can be readily computed using Eq. (6). The stepped intensity band illustrated in Fig. 2 is an example of the direct application of Eq. (6) where the height of each step is given by a single term in the summation. The 2θ position is easily obtained from Bragg's Law and data relating the lattice parameter with composition. The stepped envelope for the subband is not the measured curve because of instrumental factors which smear the band noticeably at the end points. The central region, with a slowly varying intensity, remains unaffected by instrumental broadening. The inset of Fig. 2 illustrates the normalized form for the pure instrumental broadening with only the K_{α_1} component of the $K_{\alpha_1}-K_{\alpha_2}$ doublet. A Cauchy form with an asymmetry fits the broadening function provided it is due mainly to the spectral distribution of the emission line.[8] This holds true in the early stages of diffusion if a high-resolution diffractometer is used and the crystal structure of the composite material remains relatively perfect. Under these conditions Eq. (6) can be extended to include instrumental broadening, i.e.,

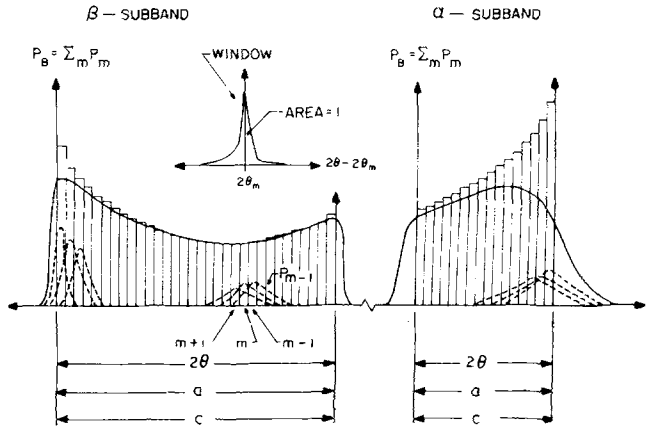

FIG. 2. Intensity subbands, consisting of summation of integrated intensities for all measurable sections of composition m (stepped curve), individual specimen broadening functions (dashed), instrumental broadening function (upper center), broadened intensity band (solid). Horizontal scale expressible in terms of diffractometer angle (2θ), lattice parameter (a), or composition (c).

$$P_B(2\theta) = I_0 g \Delta V \sum_m Q_m \left(\frac{\exp(-2\langle\mu\rangle_m Y_m/\sin\theta_m)}{\pi\Delta 2\theta'_m \sin\theta_m}\right) \times\left[1+\left(\frac{2\theta-2\theta_m}{\Delta 2\theta'_m}\right)^2\right]^{-1}, \tag{9}$$

where $\Delta V = A_0\Delta Y$. The semi-half-widths $\Delta 2\theta'_m$ (in radians) can usually be obtained only at the sharp end points where the broadening significantly influences the data. Consequently, only two Cauchy functions are necessary for each band that are characteristic of the extreme compositions. If the instrumental curves are asymmetric (which is most often true), then a pair of semi-half-widths ($\Delta 2\theta'_{mU}$ and $\Delta 2\theta'_{mL}$) are required corresponding to each extreme composition.

It was found that the broadening function can become Gaussian after longer diffusion treatments. This is related to the formation of a substructure associated with diffusion damage. Thus far, a significant strain term has not been observed, probably because of high dislocation mobility at the diffusion temperatures. Therefore, all of the broadening can be described largely by a Gaussian distribution of subgrain tilts and particle size broadening. If the latter is introduced into Eq. (6)

$$P_B(2\theta) = I_0 g \Delta V \sum_m Q_m \left(\frac{\exp(-2\langle\mu\rangle_m Y_m/\sin\theta_m)}{\beta_m \sin\theta_m}\right) \times\exp\left(-\pi\frac{(2\theta-2\theta_m)^2}{\beta_m^2}\right), \tag{10}$$

where

$$\beta_m^2 = \frac{\lambda^2}{L_{3m}^2\cos^2\theta_m} + \beta_{0m}^2, \tag{11}$$

L_{3m} is the subgrain size perpendicular to the reflecting planes, and β_{0m} is the instrumental parameter obtained before the diffusion anneals. In applying Eq. (11), the last term (β_{0m}) should be smaller than the first containing L_{3m}. The Gaussian broadening functions are symmetrical and β_m can be measured from semi-half-

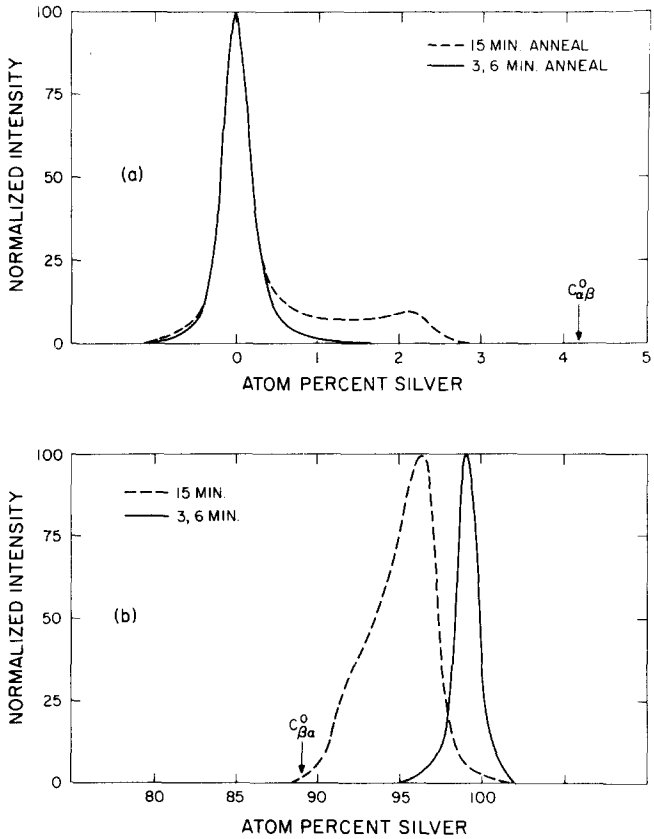

FIG. 3. Normalized (222) Cu-rich (a) and Ag-rich (b) x-ray intensity subbands after diffusing at 750 °C for 3, 6, and 15 min.

widths, $\frac{1}{2}B_m(2\theta)$, at the extremity of each intensity band using

$$\beta_m = \tfrac{1}{2}(\pi/\ln 2)^{1/2} B_m(2\theta). \tag{12}$$

Further details will be given in Sec. V.

If the composition profile is known, the intensity bands can be simulated using Eq. (9) or (10) depending upon whether the broadening is best described by a Cauchy or a Gaussian form. Usually, the composition (or lattice parameter) profile is to be determined from the intensity bands. This is carried out by trial and error estimates of the composition profile. It is helpful to recognize that reducing the slope of the composition profile results in an increase in the intensity at the corresponding 2θ points within the intensity bands. That is, there is a reciprocal relationship between the slope of the composition profile and the intensity. A computer program[9] has been written to carry out the calculations associated with Eqs. (9) and (10). Sec IV provides examples of this procedure using the Cu-Ag system.

IV. EXPERIMENTAL RESULTS FOR THE Cu-Ag SYSTEM

A specimen was prepared with a 3.2-μm electrodeposit of Ag on a (111)-oriented Cu single crystal of 99.99% purity. The Cu substrate crystal was acid cut from a $\frac{3}{4}$-in.-diam rod to a thickness of about $\frac{1}{4}$-in. and then acid polished. This resulted in a dislocation density of about $10^5/\text{cm}^2$ and (111) planes were within 1° of the surface cut.

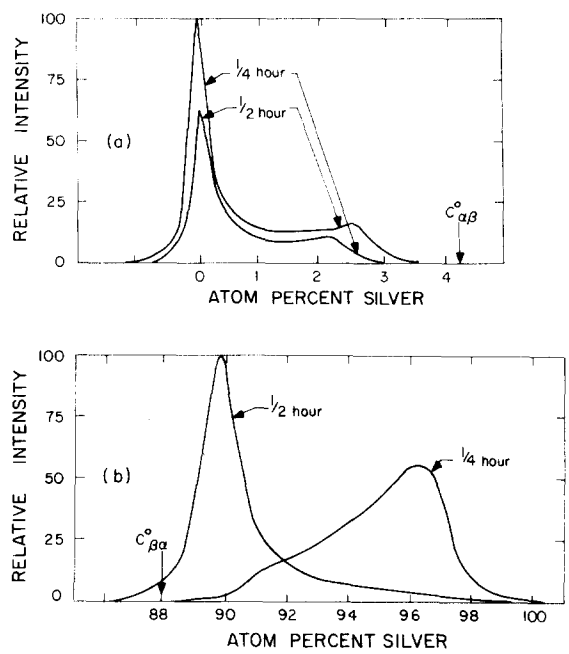

FIG. 4. (222) Cu-rich (a) and Ag-rich (b) x-ray intensity subbands after diffusing at 750 °C for 15 and 30 min.

A Siemens ω-drive diffractometer was modified to include a focusing (Jagodzinski) high-resolution monochromator. This was set up to exclude the K_{α_2} line of the $K_{\alpha_1} - K_{\alpha_2}$ doublet from a fine-focus Cu diffraction tube. Also, a 0.05-mm receiver slit was used with the tube providing a line 8×0.04 mm at the 6° take-off angle. The λ/n components were removed with a scintillation counter and a pulse height analyzer.

The Cu-Ag specimen was diffused at 750 °C for 3, 6, 15, and 30 min as well as 1, 2, and 8 h. A 10-sec correction was applied to all diffusion treatments to allow for heat-up and quenching. Figure 3 illustrates diffraction patterns plotted against percent Ag after annealing for 3, 6, and 15 min. An insignificant inten-

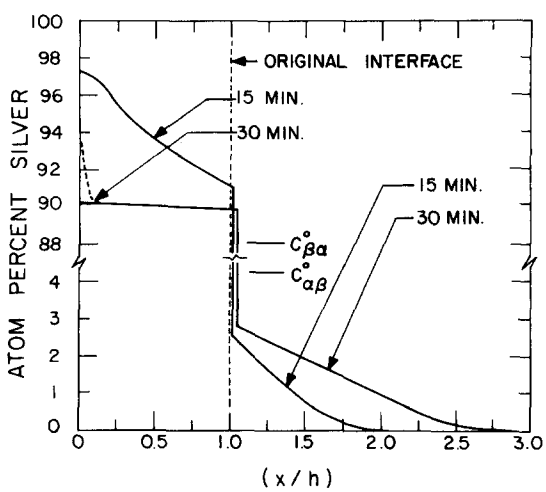

FIG. 5. Composition profiles obtained from x-ray subbands after diffusing at 750 °C for 15 and 30 min with $h \approx 3.2$ μm.

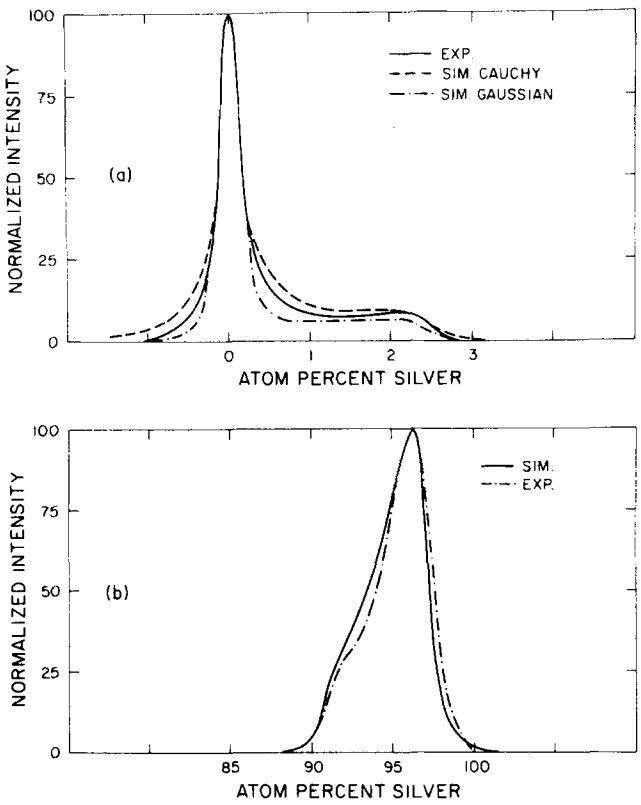

FIG. 6. Cu-rich (a) and Ag-rich (b) (222) simulated and experimental intensity subbands for diffusion at 750 °C (15 min). Curve (a) illustrates simulations with pure Cauchy and Gaussian broadening functions, while (b) contains a pure Gaussian simulation.

sity change was found after the 3- and 6-min anneals with no measurable subband formation. However, subband formation was found in the diffraction pattern after 15 min of diffusion. Figure 4 illustrates large changes in the intensity subbands after 15—30 min. The intensity distributions broaden and are seen to cut off at higher solubility limits with additional diffusion time. If the diffusion time is extended up to 8 h, the intensity cutoff approaches but still remains below the solubility limits ($C^0_{\alpha\beta}$ and $C^0_{\beta\alpha}$) given in the equilibrium diagram[10] at 750 °C.

By using a computer simulation program[9] for each subband, the composition profiles illustrated in Fig. 5 are obtained. The variation of lattice parameter with composition is required; however, this is already available in the literature.[11] After only 15 min of diffusion, stage II[7] is attained. After 30 min, diffusion has proceded to stage III and the measured solubilities for the Ag-rich plating at each time are 91.0 and 89.6% Ag, while for the Cu-rich phase they are 2.5 and 2.8% Ag. The maximum solubilities observed after further annealing at 750 °C are 11.4% Cu in the Ag-rich phase and 3.2% Ag in the Cu-rich phase. The first number is close to the value 11.9% Cu obtained from the equilibrium diagram, while the second is 1% smaller than the corresponding equilibrium value (4.2%). Such differences are not surprising when diffusion times are short as is the case for small diffusion couples.

Figures 6 and 7 illustrate the fit obtained between the experimental intensity bands and the computer simulations obtained from the composition profiles of Fig. 5 Simulations were carried out for both the Cauchy and Gaussian broadening functions which are illustrated in Fig. 6(a). It can be seen that the experimental curve is intermediate between both simulations indicating that a small amount of particle size broadening has been introduced after 15 min of diffusion. Before annealing, the shape of the Cu reflection is closer to the Cauchy form. A Gaussian form has been used in the simultation of Fig. 6(b). Figures 7(a) and 7(b) illustrate experimental results and simulations after $\frac{1}{2}$ h of diffusion. An examination of Fig. 7(b) illustrates that the experimental curve displays an asymmetry not included in the similation. In the preliminary simulations, the asymmetry was fitted (see dashed line of Fig. 5). However, this is not a likely distribution for Ag. Such an asymmetry can result from an expansion of the diffraction planes near the free surface due to hydrocarbons introduced near the surface from incomplete trapping of diffusion pump oil. Such an effect has been observed in the case of vacuum-annealed tungsten by one of the authors. In the present case, the specimen was vacuum encapsulated in quartz using an oil diffusion pump. It is likely that thelarger interplanar spacing results from a small amount of hydrocarbons located near the surface rather than an enrichment of the larger Ag atoms. Subsequent diffusion anneals also show a similar asymmetry which is not due to Ag enrichment. This interpretation was confirmed with ion scattering spectros-

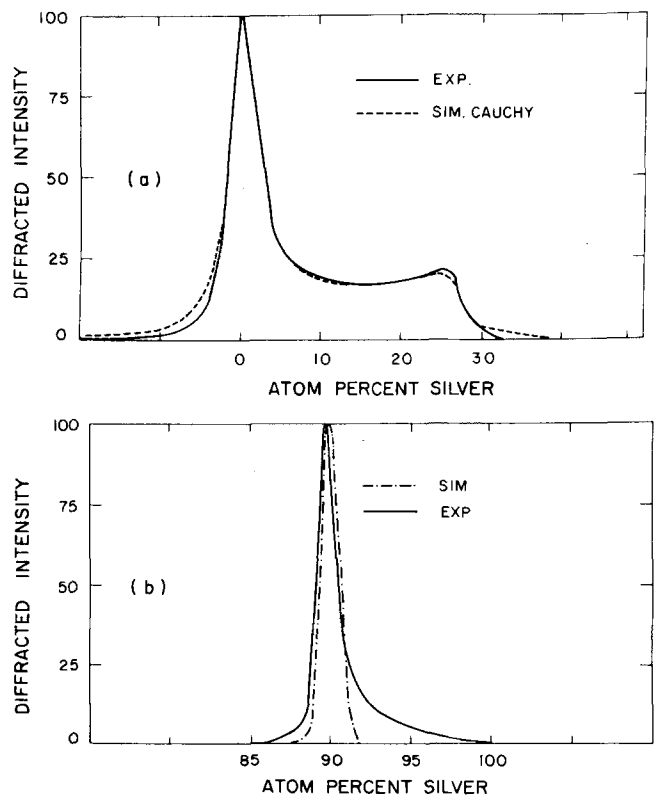

FIG. 7. Cu-rich (a) and Ag-rich (b) (222) simulated and experimental intensity subbands for diffusion at 750 °C (30 min). Curve (a) contains a Cauch broadening function, while (b) contains a Gaussian function.

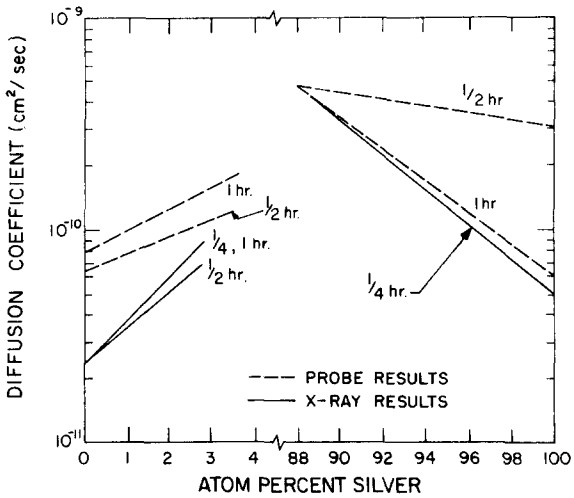

FIG. 8. Semilog plots of diffusion coefficients used to simulate the concentration profiles deduced from x-ray and probe data.

copy and EDAX results. Consequently, the true composition profile in the Ag-rich phase has been taken to be an extrapolation of the lower level Ag concentration curve extended to the free surface.

The diffusion coefficients associated with the profiles of Fig. 5 are given in Fig. 8. These were obtained using an iterative approach described in the preceding paper.[7] Coefficient curves, $D(C)$, can be obtained for each phase provided that the composition profile has not completely flattened. It was important to recognize that within the first 10 min of diffusion the interface compositions, $C_{\beta\alpha}$ and $C_{\alpha\beta}$, remained close to pure Ag and Cu. After 10 min, the interface compositions adjusted rapidly to values which approach the equilibrium concentrations. Consequently, an incubation time of 10 min must be subtracted, because only the diffusion-controlled stages are under consideration here.

Additional data were collected using the electron microprobe in order to provide a check on the diffusion coefficients. In this study, 15 μm of Ag was deposited on a $\frac{3}{4}$-in.-diam Cu single crystal which was sectioned along the cylinder axis or perpendicular to the plating into four pieces using an Isomet abrasive cutoff wheel. A separate piece was diffused for the following times: $\frac{1}{2}$, 1, 2, and 4 h at 750 °C and the surface layer was removed. The Cu K_α and Ag L_α lines were recorded as a function of distance from the diffused specimens as well as from Ag and Cu standards. Rucklidges[12] electron microprobe program (EMPADR VII) was used to convert the intensities into atom fraction of Ag. This program takes care of absorption, fluorescence, the background correction, and standardization. Figure 9 illustrates the results for the first two times which give the largest variation in β-phase composition. If these are fitted using the previously described iterative solution, $D(C)$ curves are obtained which are given in Fig. 8. The averages are shown in Fig. 10 for each phase and both methods along with other data found in the literature. An examination of the coefficients for the Ag-rich phase shows that the average value for the probe data is in good agreement with the average of the Cahoon *et al.*[13] data, while the average for x-ray results agree very well with Barreau *et al.*[14] Both the probe and x-ray results indicate that the diffusion coefficients increase with the addition of Cu. This is not surprising since the solidus temperature decreases with Cu content. For the Cu-rich phase, there is a tendency for our probe and x-ray results to average on the low side, i.e., the probe data is now below the data of Cahoon *et al.*[13] and averages close to the data of Barreau[14] and Oikawa.[15] The results of Kubaschewski[16] are on the high side of the data distribution, while the x-ray data give diffusion coefficients about one-half that obtained with the probe. This is not surprising because of the additional defects introduced in cutting the probe specimens. The x-ray specimens were prepared by acid cutting and polishing

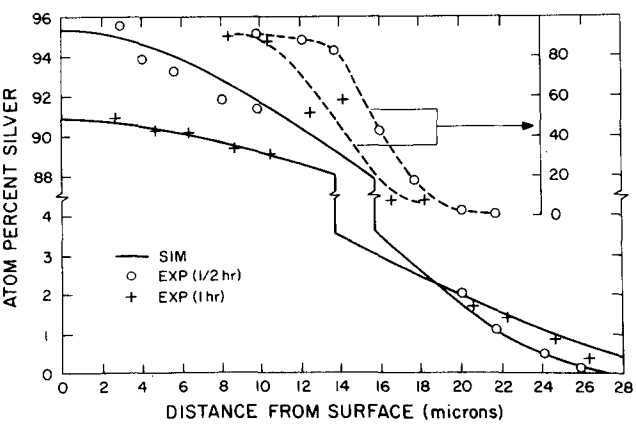

FIG. 9. Concentration profiles obtained from probe data for $\frac{1}{2}$ and 1 h at 750 °C. The solid curves are generated from the diffusion data of Fig. 8. The upper right-hand curves contain points used to determine interface position and are read to the right.

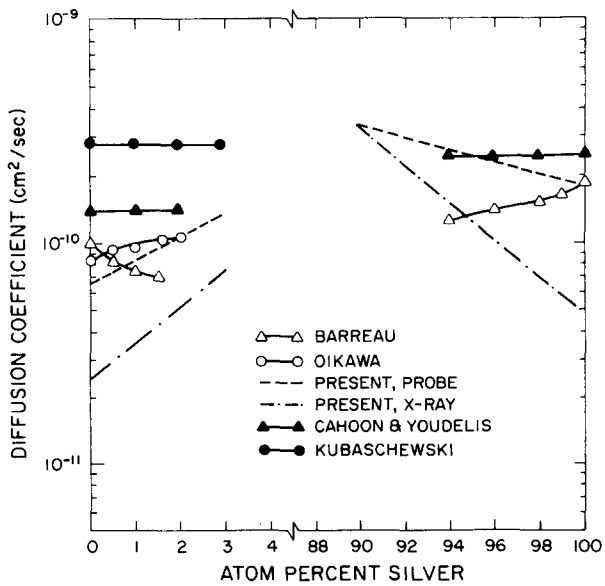

FIG. 10. Semilog plots of average diffusion coefficients obtained from the present x-ray and probe data compared with literature values.

and were never subjected to an abrasive cutting operation. Any additional defects occurred as a result of the diffusion process itself.

V. SUBGRAIN SIZE AND MISORIENTATION

Information about subgrain size L_{1m} parallel to the free surface as well as the degree of crystal misorientation can be obtained from rocking curves. Rocking curves are obtained by fixing 2θ at various compositions m along both subbands and rotating the crystal about an axis perpendicular to the plane containing the incident and diffracted beams (ω). ω is taken to be zero when the angle of incidence equals the angle of reflection θ. In previous studies of the CuNi,[3] CuAu,[17] and CuPd[5] systems, the rocking curve half-widths are often greater than 1° after correcting for instrumental broadening. This is to be compared with an instrumental half-width as small as 0.04° for the (111) and 0.08° for the (222) reflections. The additional ω line broadening represents a sizable effect which has been attributed to subgrain misorientation and particle size.[18] The broadened half-width, $B_{1m}(\omega^\circ)$, the misorientation half-width, $B_{tm}(\omega^\circ)$, the intrumental half-width, $B_{0m}(\omega^\circ)$ (all expressed in degrees) and the subgrain size, L_{1m} are related by

$$B_{1m}^2(\omega^\circ) = \frac{7.24\times10^2\lambda^2}{L_{1m}^2\sin^2\theta_m} + B_{tm}^2(\omega^\circ) + B_{0m}^2(\omega^\circ). \tag{13}$$

The particle size and tilt half-widths are separated by making half-width measurements on two orders, i.e., (111) and (222), as well as the instrumental half-width. For the Cu-Ag system, the over-all half-widths are in the vicinity of 0.50°. Although this is considerably greater than instrumental (0.06°), it is only about one-fifth of the broadening found in recent studies of the Cu-Ni system. An average value of $\langle L_{1m}\rangle = 254$ Å has been found for the Ag-rich phase and 470 Å was found for the Cu-rich phase. The average misorientation half-widths, $\langle B_{tm}(\omega^\circ)\rangle$, were 0.48° and 0.36° for the Ag- and Cu-rich phases with the Cu-rich phase remaining more perfect than the Ag-rich plating at all times.

The particle size along the diffusion direction can be obtained from the Scherrer equation[18,19] combined with instrumental broadening

$$B_{3m}^2(2\theta^\circ) = \frac{2.90\times10^3\lambda^2}{L_{3m}^2\cos^2\theta_m} + B_{0m}^2(2\theta^\circ). \tag{14}$$

Equation (14) requires $B_{3m}(2\theta^\circ)$, the broadened half-width and $B_{0m}(2\theta^\circ)$, the instrumental half-width, all in degrees. As previously stated, it is necessary to obtain the semi-half-widths $\frac{1}{2}B_m(2\theta^\circ)$ from the extreme ends of each intensity band, because measurements within the intensity bands are likely to be influenced by composition broadening. An average $\langle L_{3m}\rangle$ value of 1698 Å is obtained for the Cu-rich phase, while the corresponding average for Ag-rich phase is 1015 Å. The large number for the Cu-rich phase may contain a sizable error since the line broadening is small.

It is interesting to consider the subgrain shape factor $\langle L_{3m}\rangle/\langle L_{1m}\rangle$ for each phase. This ratio is 3.6 for the Cu-rich phase and 4.0 for the Ag-rich phase. The latter is very close to the ratio of the plating thickness to the grain size of the Ag-rich deposit. Consequently, the subgrain shape factor appears to be determined by the macroscopic dimensions of the grains within the plating. The Cu-rich phase began with a higher degree of perfection and remained more perfect after extensive diffusion treatments. Also, there was a tendency for the rocking curves to be somewhat broader near the free surface than at the interface.

VI. SUMMARY

A computer program was used to obtain composition profiles from the x-ray intensity subbands for the Cu-Ag system. This is carried out by trial and error with the composition profiles systematically refined until the experimental intensity band shapes are fitted. It is assumed that the variation of lattice parameter with composition is known. Small changes in the lattice parameter profile shape produce large changes in the x-ray simulations because the latter depend upon the first derivitive of the lattice parameter profile. The computer program used for these simulations will be made available as an NTIS report.[9]

An iterative approach has been applied to determine the diffusion coefficients for each phase as a function of composition. A given coefficient curve is obtained by assuming an initial curve and refining its shape until the experimental composition profiles have been fitted. The procedure requires very little computer time since the iterative approach converges rapidly. This computer program will also be made available through a second NTIS report.[20] It was found that diffusion coefficients obtained using the electron microprobe were within a factor of 2 of those obtained from the x-ray data. The higher values for the probe data can be explained by differences in specimen preparation. All of the diffusion coefficients which we obtained increase as the interface compositions are approached. This trend is in accord with the decrease in solidus temperature found as the solute content for each phase is increased. Since the diffusion coefficients for both phases are close to 10^{-10} cm^2/sec at 750 °C and the solubility of the Ag-rich phase is about three times that for the Cu-rich phase, the initial interface movement is toward the substrate with reversal occurring at a later time.

In these studies, the diffusion couple consisted of a 3.2 μm of Ag on a large Cu substrate and represents a semifinite system with correspondingly short diffusion times. The earliest stages of an interface reaction become more apparent with a shortened experimental time scale. It was found that the limiting solubilities associated with the equilibrium diagram were not approached until after 10 min of diffusion. After this initial period the limiting solubilities quickly approached the equilibrium values. However, the values found within an 8-h diffusion treatment at 750 °C were always less than the equilibrium solid solubilities at this temperature. This is especially true for the Cu-rich phase.

Previous x-ray investigations as well as the present study of the Cu-Ag system, have demonstrated that atomic diffusion generates a substructure. This diffusion damage was found to be much smaller for the Cu-Ag

system than for small couples containing Ni, Pd, or Au deposits on Cu. The average subgrain size is smaller in the Ag-rich phase than in the Cu-rich phase. Also, a larger average crystal misorientation (tilt) is found in the Ag-rich phase. Subgrain shapes can be compared by taking the ratio of the subgrain size along the interface normal to the size in a perpendicular direction. The subgrain shape factor within the plating corresponds to the ratio of the plating thickness to the optical grain size obtained in the early stages of diffusion. This relationship also holds for the Cu-Ni system.

All of the findings for the Cu-Ag couples diffused at 750 °C are compatible with a one-dimensional planar diffusion model. This is reasonable since the ratio of absolute diffusion temperature to the eutectic temperature is 0.97 which corresponds to a high relative temperature. Although lattice diffusion is expected to be dominant, there are indications that high-diffusivity paths are operative within the grains especially for the probe samples which were initially cut with a diamond wheel. However, in either case a one-dimensional volume diffusion model appears to be satisfactory.

ACKNOWLEDGMENT

The authors are grateful to the National Science Foundation for funding this research.

[1]C.R. Houska, J. Appl. Phys. **41**, 69 (1970).
[2]D.R. Tenney, J.A. Carpenter, and C.R. Houska, J. Appl. Phys. **41**, 4485 (1970).
[3]J.A. Carpenter, D.R. Tenney, and C.R. Houska, J. Appl. Phys. **42**, 4305 (1971).
[4]C.R. Houska, High Temp.-High Pressures **4**, 417 (1972).
[5]D.R. Tenney and P.K. Talty, Metall. Trans. **5**, 241 (1974).
[6]J. Unnam, J.A. Carpenter, and C.R. Houska, J. Appl. Phys. **44**, 1957 (1973).
[7]C.R. Houska and J. Unnam, preceding paper, J. Appl. Phys. **47**, 4325 (1976).
[8]E.R. Pike, Acta Crystallogr. **12**, 87 (1959).
[9]J. Unnam, D.R. Tenney, J.A. Carpenter, and C.R. Houska, College of Engineering, Virginia Polytechnic Institute and State University, Technical Report No. VPI-E76.9, 1976, available from the National Technical Information Service, Springfield, Virginia.
[10]M. Hansen, *Constitution of Binary Alloys* (McGraw-Hill, New York, 1958).
[11]W.B. Pearson, *A Handbook of Lattice Spacings and Structures of Metals and Alloys* (Pergamon, London, 1958), Vol. I; *ibid.* (1967), Vol. 2.
[12]J. Rucklidge and E.L. Gasparrini, EMPADR-VII, University of Toronto, Department of Geology (unpublished).
[13]J.R. Cahoon and W.V. Youdelis, Trans. Metall. Soc. AIME **239**, 127 (1967).
[14]G. Barreau, G. Brunel, G. Cizeron, and P. Lacombe, Mem Sci. Rev. Metall. **68**, 357 (1971).
[15]H. Oikawa, H. Takei, and S. Karashima, Metall. Trans. **4**, 653 (1973).
[16]O. Kubaschewski, Trans. Faraday Soc. **46**, 713 (1950).
[17]D.R. Tenney (unpublished).
[18]C.R. Houska, Thin Solid Films **25**, 451 (1975).
[19]B.E. Warren, *X-Ray Diffraction* (Addison-Wesley, Reading, Penna., 1969), pp. 251—313.
[20]J. Unnam and C.R. Houska, College of Engineering, Virginia Polytechnic Institute and State University, Technical Report No. VPI-E76.3, 1976, available from the National Technical Information Service, Springfield, Virginia.